

# Assembly of Surface-Confined Homochiral Helicates: Chiral Discrimination of DOPA and Unidirectional Charge Transfer

Revital Kaminker,<sup>†</sup> Xavier de Hatten,<sup>‡</sup> Michal Lahav,<sup>†</sup> Fabio Lupo,<sup>⊥</sup> Antonino Gulino,<sup>⊥</sup> Guennadi Eymenenko,<sup>§,||</sup> Pulak Dutta,<sup>§</sup> Colm Browne,<sup>‡</sup> Jonathan R. Nitschke,<sup>\*,‡</sup> and Milko E. van der Boom<sup>\*,†</sup>

<sup>†</sup>Department of Organic Chemistry, The Weizmann Institute of Science, 76100 Rehovot, Israel,

<sup>‡</sup>Department of Chemistry, University of Cambridge, Lensfield Road, Cambridge CB2 1EW, United Kingdom

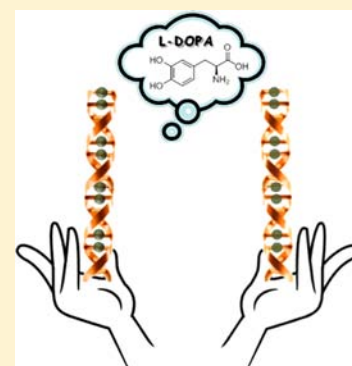
<sup>§</sup>Department of Physics and Astronomy, Northwestern University, Evanston, Illinois 60208-3112, United States,

<sup>||</sup>Department of Materials Science and Engineering, Northwestern University, Evanston, Illinois 60208-3108, United States, and

<sup>⊥</sup>Dipartimento di Scienze Chimiche, Università di Catania, Catania 95125, Italy

## Supporting Information

**ABSTRACT:** Surface-confined double-helical polymers are generated by dynamic covalent assembly with preservation of chirality, metal coordination environment, and oxidation state of the precursor complexes. This one-step procedure involves both in solution and solution-to-surface assembly and resulted in chiral interfaces where pairs of ligands are wrapped around arrays of metal ions. In-plane XRD experiments revealed the formation of a highly ordered structure along the substrate surface. The chirality of the surfaces is expressed by the selective recognition of 3,4-dihydroxyphenylalanine (DOPA). The CD measurements show a response of the  $\Delta$ -polymer-modified quartz substrates toward D-DOPA, whereas no change was observed after treatment with L-DOPA. These coordination-based interfaces assembled on metal-oxide substrates in combination with a redox-probe,  $[\text{Os}(\text{bpy})_3](\text{PF}_6)_2$ , in solution can resemble the behavior of a rectifier.



## INTRODUCTION

The assembly of metal–organic systems in solution and their associated studies have had a tremendous impact on many aspects of chemistry.<sup>1,2</sup> The attachment of such well-defined molecular architectures to surfaces is generating much attention,<sup>3</sup> partly because of their potential uses in electronic and other devices.<sup>4</sup> The stepwise solid-state generation of metal–organic systems from solution has resulted in highly ordered structures,<sup>5</sup> which are impossible to form or are not readily attainable by other methods. An important aspect of surface-functionalization is chirality. Chiral films have been used for discriminative sensing of enantiomers as shown by Wöll and Fischer with Metal–Organic Frameworks (MOFs)<sup>6</sup> as well as to address questions related to biological homochirality and the origin of life.<sup>7</sup> The formation and characterization of chiral interfaces with additional built-in functionalities such as redox-active and structurally demanding metal centers is scientifically challenging because of their high molecular complexity and versatility. Such redox-active interfaces may display unique and useful electron transfer (ET) processes.<sup>8</sup>

We demonstrate here the self-assembly of surface-confined double-helical polymers in which pairs of self-assembled ligands are wrapped around an array of copper(I) ions. Incubation of hydrophilic and hydrophobic substrates in a solution of subcomponents led to the formation of surface-bound extended

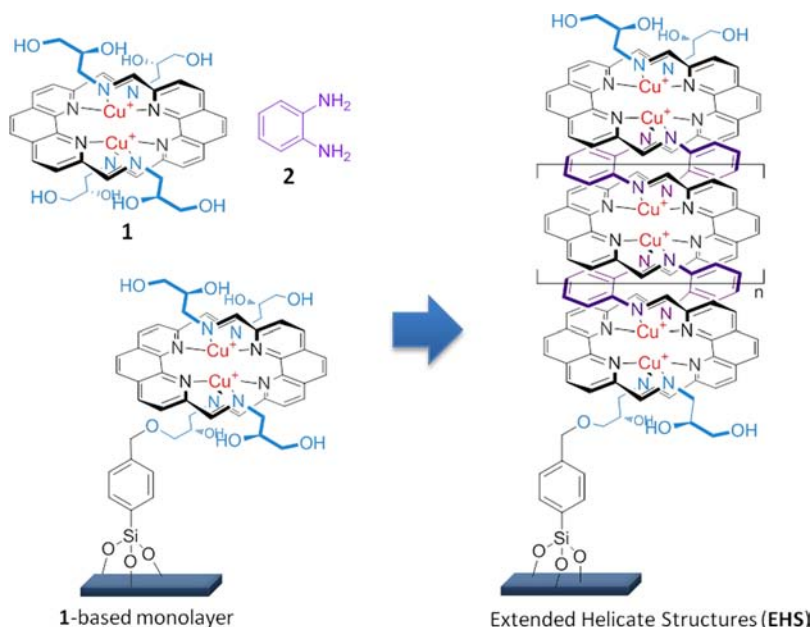
helical structures (EHS). Our assembly process transfers the chiral structure ( $\Lambda$  or  $\Delta$ ) of individual copper complexes (**1**)<sup>9</sup> from solution into surface-bound extended EHS. These unique structures were generated through the reaction of dicopper double-helicate **1**<sup>9b</sup> and 1,2-diaminobenzene (**2**). The primary structure is a function of the metal–ligand coordination chemistry, whereas the oligomeric structure is a result of dynamic-covalent assembly.<sup>10</sup> The monolayer of the copper complex **1** and the EHS have strikingly different electrochemical (EC) properties with the EHS setup resembling the behavior of a rectifier. Moreover, the EHS showed enantioselective interactions with 3,4-dihydroxyphenylalanine (DOPA) as demonstrated by circular dichroism (CD) of the thin films (Scheme 1).

## RESULTS AND DISCUSSION

The **1**-based monolayer was prepared through the reaction of *p*-iodobenzyl functionalized quartz, ITO and silicon substrates with the  $\Lambda$ -derivative of helicate **1** at 50 °C for four days under an inert atmosphere with exclusion of light (see the Supporting Information, SI, and Scheme S1 for details).<sup>9,11</sup> Subsequently, the functionalized substrates were thoroughly washed with

Received: July 26, 2013

Published: October 8, 2013

Scheme 1. Multicomponent Assembly of the Chiral Extended Helicate Structures (EHS) in Water<sup>a</sup>

<sup>a</sup>The monolayer is formed through reaction of a *p*-iodobenzyl-functionalized surface with helicate **1** (Supporting Information Scheme S1).<sup>9,11</sup>

sonication in organic solvents to remove possible physisorbed material. The monolayer was not removed by abrasion with ethanol-wetted Kimwipe tissues, demonstrating that these films are strongly bound to the substrate surfaces.

Structural information of the 1-based monolayer on silicon substrates was obtained by synchrotron X-ray reflectivity (XRR) measurements, X-ray photoelectron spectroscopy (XPS) analysis, and semicontact atomic force microscopy (AFM). Transmission UV/vis spectroscopy and cyclic voltammetry were used to analyze the films formed on quartz and ITO, respectively. UV/vis spectroscopy of the 1-based monolayer shows a spectrum having two main bands at  $\lambda = 227$  and 290 nm (Figure 1A, lower trace). Similar absorptions were observed for **1** in solution,<sup>9b</sup> indicating that the molecular structure of the surface-bound helicate is intact.

The XRR measurements indicated a film thickness on silicon substrates of 1.9 nm and a surface roughness of 0.5 nm (Figure 2A).<sup>12</sup> The XRR-derived average molecular footprint is  $\sim 0.7$  nm<sup>2</sup>, indicative of the formation of a densely packed structure. The observed thickness for the 1-based monolayer is as expected, considering the thickness of the *p*-iodobenzyl-based monolayer (0.7 nm) and the estimated molecular dimensions of helicate **1** (0.8 nm  $\times$  1.2 nm). Angle-resolved XPS atomic concentration analysis revealed N/Cu ratios of 3–4, which reflects the expected elemental stoichiometry (as was observed by powder XPS analysis of helicate **1**).<sup>13</sup> Two signals were observed at 932.5 and 952.4 eV, indicative of Cu<sup>I</sup> (Figure 2B). AFM imaging shows a relatively smooth and mostly homogeneously covered surface on silicon with some minor defects (SI Figure S1). For instance, scan areas of 500 nm  $\times$  500 nm have a root-mean-square roughness ( $R_{\text{rms}}$ ) of only 0.25 nm.

The EHS were generated by treating the monolayer prepared from helicate **1- $\Lambda$**  with an aqueous solution containing the same enantiomer of **1** (0.40 mM) and 1,2-diaminobenzene (3.70 mM; Scheme 1). The multicomponent assembly process was carried out in sealed glass tubes at 50 °C for five days under an inert atmosphere with the exclusion of light. The resulting films were briefly sonicated in water and ethanol, and then dried under a stream of N<sub>2</sub>. The EHS were characterized by the same methods as for the monolayer. In addition, we used also in-plane XRD and circular dichroism (CD) spectroscopy. The latter method provided strong evidence of the formation of the chiral EHS- $\Lambda$  (vide infra). The XRR measurements indicated a film thickness on silicon substrates of 10 nm, consistent with an average EHS length of  $\sim 26$  Cu<sup>I</sup> ions (for the case where the chains are orthogonal to the surface), and a surface roughness of 1.4 nm (Figure 3A). The increase in film thickness in this assembly process is significant ( $>10\times$ ). No Bragg peak is observed in the perpendicular direction to the substrate. The absence of electron density oscillations indicate the formation of a uniform structure (Figure 3A, inset). An electron density comparison suggests that the EHS density follows the

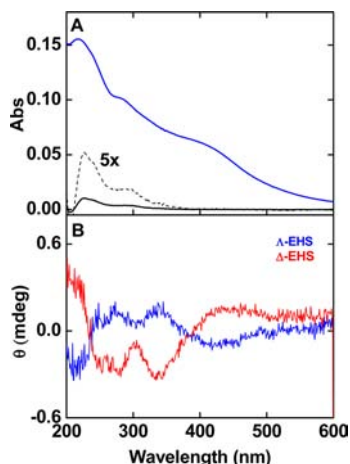


**Figure 1.** (A) UV/vis absorption spectra for the EHS- $\Lambda$  (blue line) and the 1-based monolayer (black line) on quartz substrates. The dotted line is the magnified monolayer spectrum. (B) CD spectra for  $\Lambda$  (blue) and  $\Delta$  (red)-based EHS.

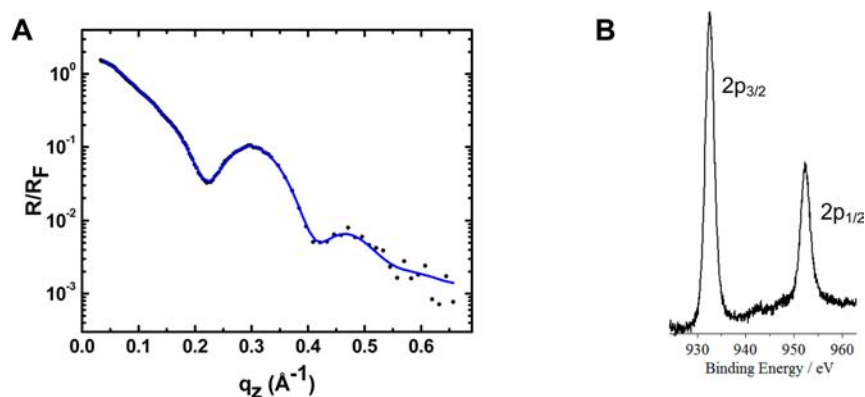


**Figure 2.** (A) Synchrotron X-ray reflectivity (XRR) spectrum of the **1**-based monolayer on a silicon substrate. The blue trace is a fit to the experimental data.<sup>12</sup> (B) Monochromatized Al- $K\alpha$  XPS spectrum for the **1**-based monolayer in the Cu 2p binding energy region.

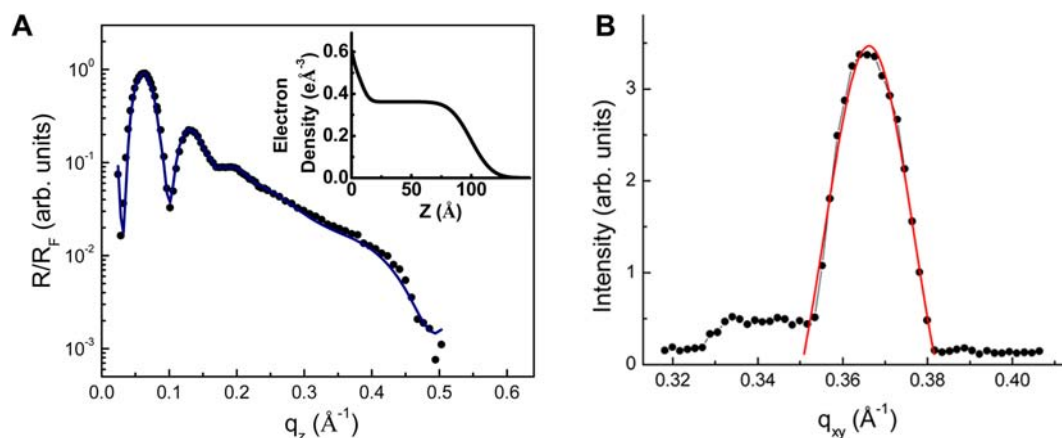


**Figure 3.** (A) Normalized specular X-ray reflectivity pattern of EHS. The black trace is a fit to the experimental data.<sup>12</sup> The corresponding electron density profile is shown in the inset. (B) In-plane XRD analysis showing a diffraction peak at  $q_{xy} = 0.366 \text{ \AA}^{-1}$ .

molecular footprint of the monolayer, as expected for a near-quantitative coupling process. Interestingly, in-plane XRD measurements show a Bragg peak that corresponds to lateral ordering of  $17.3 \text{ \AA}$  with correlation length of  $\sim 22 \text{ nm}$ , demonstrating the formation of a highly ordered structure along the substrate surface (Figure 3B). Such observations are rare for molecular assemblies.<sup>14</sup> The correlation length is in good agreement with the domains having a diameter of  $\sim 20 \text{ nm}$  observed by AFM (Figure 4). The successful covalent coupling of the three components (**1**, **2** and the **1**-based monolayer) was further confirmed by angle-resolved XPS

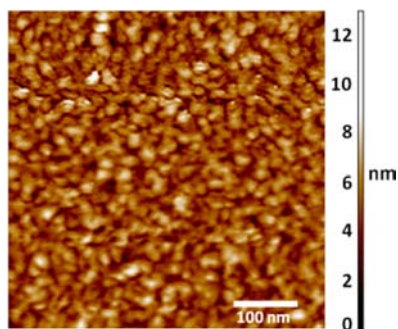


**Figure 4.** Representative atomic force microscopy (AFM) topography image of the EHS on a silicon substrate with a root-mean square roughness ( $R_{\text{rms}}$ ) of  $1.2 \text{ nm}$ . The domains have a diameter of  $\sim 20 \text{ nm}$ .

atomic concentration analysis, which revealed an N/Cu ratio of  $\sim 3.5$ , which approaches the ideal ratio of 4 (as was observed by powder XPS analysis of helicite **1**). The XRR and AFM surface roughness suggest a low polydispersity.

The UV/vis spectrum of the EHS on quartz substrates shows three bands at  $\lambda = 218, 280, \text{ and } 400 \text{ nm}$  (Figure 1A, upper trace). The two high-energy bands are hypsochromically shifted ( $\Delta\lambda = 10 \text{ nm}$ ) in comparison with the bands of the **1**-based monolayer. We attribute the band at  $\lambda = 400 \text{ nm}$  to a metal-to-ligand charge-transfer (MLCT). These observations are characteristic for the formation of an EHS in solution and in agreement with computational studies.<sup>9a</sup> The EHS absorption intensities are  $\sim 15$  times larger than those observed for the **1**-based monolayer, which mirrors the degree of increase of film thicknesses of EHS vs the monolayer.<sup>15</sup> CD measurements unambiguously revealed the chiral nature of the EHS (Figure 1B). The CD spectrum for the EHS- $\Lambda$  is similar to the solution spectrum of helicite **1**- $\Lambda$ .<sup>9b</sup> The spectrum of this surface-confined EHS shows features with positive Cotton effects at  $\lambda = 247, 271, \text{ and } 335 \text{ nm}$ , negative Cotton effects at  $\lambda = 213, 305, \text{ and } 443 \text{ nm}$ , and crossovers at  $\lambda = 236 \text{ and } 384 \text{ nm}$  (Figure 1B, blue spectrum). To verify our findings, we also prepared the  $\Delta$ -based EHS using a monolayer of helicite **1**- $\Delta$  on quartz. In this case, CD measurements showed the mirror-image spectrum (Figure 1B, red spectrum). Interestingly, the EHS- $\Lambda$  is also formed by treating the monolayer prepared from helicite **1**- $\Lambda$  with an aqueous solution containing the three components that generate complex **1**- $\Lambda$ : 1,10-phenanthroline-2,9-dicarboxal-

hyde (1.7 mM), (S)-3-amino-1,2-propanediol (8.0 mM) and  $\text{Cu}(\text{MeCN})_4\text{BF}_4$  (1.9 mM). Heating this mixture for five days at 50 °C under  $\text{N}_2$  in the presence of 1,2-phenylenediamine (3.4 mM) with the exclusion of light also generates the EHS- $\Lambda$  as judged by UV/vis and CD spectroscopy, ellipsometry and AFM imaging (SI Figures S3–S5). Similar EHSs were obtained from helicate 1- $\Lambda$  and 1,2-diaminobenzene with bare hydrophilic substrates or silicon and quartz substrates functionalized with hydrophobic pentyl-siloxane monolayers (SI Figures S6,S7).

The homochirality of the EHSs is expressed by enantioselective interactions with a well-known neurotransmitter (DOPA). The  $\Delta$ -EHS-modified quartz substrates were immersed in a solution of D-DOPA or L-DOPA (2.5 mM) for 15 min (in a phosphate buffer solution, 0.1 M, pH 7.4) followed by rinsing with water and drying under a stream of nitrogen. The CD measurements show a clear response of the system toward D-DOPA, whereas no change in spectrum was observed after treatment with L-DOPA (Figure 5).

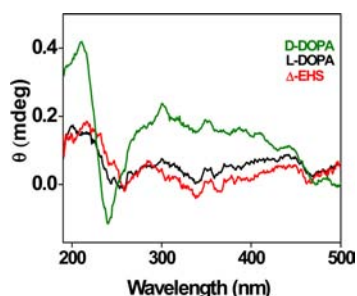


**Figure 5.** CD spectra for the  $\Delta$ -EHS functionalized substrate treated with a phosphate buffer solution (0.1 M, pH 7.4) without DOPA (red) and with L-DOPA (black) or D-DOPA (green) (2.5 mM) for 15 min followed by rinsing with water and drying under a stream of nitrogen.

The electrochemical properties of the 1-based monolayer and the EHS were studied by cyclic voltammetry (Figure 6). While quasi-reversible behavior ( $E_a = -0.081$  V,  $E_c = -0.197$  V,  $\Delta E = 0.116$  V) is observed for the 1-based monolayer, an irreversible process ( $E_a = 0.188$  V,  $E_c = -0.094$  V,  $\Delta E = 0.282$  V) is observed for the EHS.<sup>7a</sup> The increase in current density and the broadening of peak potentials for the surface-confined

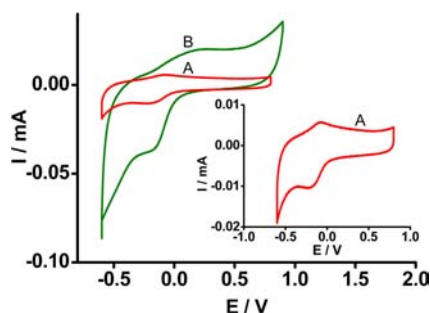


**Figure 6.** Cyclic voltammograms (CVs) of (A) the 1-based monolayer, and (B) the extended helicate structure (EHS) on double-sided ITO-coated glass. Multicyclic voltammetry results for the EHS are shown in SI Figure S13. Inset: magnification of voltammogram A. The experiments were performed at room temperature in a phosphate buffer electrolyte solution (0.1 M, pH 7.4) after degassing with argon. Pt wire and Ag/AgCl were used as counter and reference electrodes, respectively. Scan rate: 100  $\text{mVs}^{-1}$ .

EHS are attributed to the formation of a structure composed of  $\text{Cu}^{\text{I}}$  redox centers. These metal centers are spaced at different distances from the electrode surface having therefore, different electron transfer (ET) characteristics.<sup>16a</sup> Linear relationships ( $R^2 \geq 0.98$ ) were obtained for redox peak currents vs scan rates for both the 1-based monolayer and the EHS. These observations indicate that the redox processes involving the copper centers are surface-confined and electron transport is not limited by diffusion (SI Figure S8).<sup>16b</sup> Electrochemical experiments were also performed in argon-degassed  $\text{KNO}_3$  electrolyte solutions to evaluate possible complexation of the copper ions by the phosphate buffer. Although some differences were observed, ligation of the copper ions by phosphate anions is not evident (SI Figure S12).

The ET properties of our helical assemblies were studied using EHS modified ITO electrodes and  $[\text{Os}(\text{bpy})_3](\text{PF}_6)_2$  as a redox-probe in solution. ET between redox-probes and electrodes functionalized with thin films might involve (i) a diffusional pathway, where a probe reacts at the ITO–solution interface or (ii) a charge transfer pathway, where the probe is oxidized at the film–solution interface.<sup>17</sup> For pathway II, the charge transfer can involve an irreversible oxidation of the probe by the film. The CVs of  $[\text{Os}(\text{bpy})_3](\text{PF}_6)_2$  (50  $\mu\text{M}$  in a phosphate buffer) recorded with a bare ITO electrode or an ITO electrode functionalized with a 1-based monolayer showed the reversible redox characteristics of an  $\text{Os}^{\text{II/III}}$  couple with  $E_{1/2} = 0.656$  V ( $Q = 4 \times 10^{-6}$  C). The monolayer does not seemingly affect the ET processes (Figure 7), indicating that

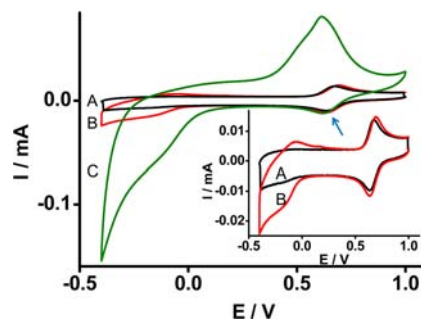


**Figure 7.** Cyclic voltammograms (CVs) of  $[\text{Os}(\text{bpy})_3](\text{PF}_6)_2$  (50  $\mu\text{M}$ ) in solution: (A) bare ITO electrode, (B) ITO substrates functionalized with the 1-based monolayer, and (C) the EHS. Inset: Magnification of CVs A and B. The measurements were performed at rt in an argon-degassed phosphate buffer solution (0.1 M, pH 7.4 vs Ag/AgCl) at 100  $\text{mVs}^{-1}$ . Differential pulse voltammograms (DPVs) and CVs at different scan rates (25–700  $\text{mVs}^{-1}$ ) are shown in SI Figures S9–S11.

the redox-probe can readily reach the ITO surface. In contrast, the CVs of  $[\text{Os}(\text{bpy})_3](\text{PF}_6)_2$  recorded with an ITO electrode functionalized with the EHS showed an irreversible process with a significantly amplified (7-fold,  $Q = 2.8 \times 10^{-5}$  C) anodic wave, and an essentially unchanged cathodic signal ( $Q = 3.8 \times 10^{-6}$  C).

The anodic wave consists of two overlapping oxidation peaks that were clearly distinguished by differential pulse voltammetry, DPV (SI Figure S9–S10). The oxidation current can be attributed to: (i)  $\text{Os}^{\text{II}}$  direct diffusion to the ITO, and more importantly to (ii) ET from the  $\text{Os}^{\text{II}}$  complexes ( $E_a = 0.644$  V) in solution to the surface-confined  $\text{Cu}^{\text{II}}$  ions ( $E_a = 0.188$  V). The large “electroactive” surface-area of the EHS is likely to enhance the ET between the diffusional  $\text{Os}^{\text{II}}$  species and the ITO electrode, through the multiple copper centers of the EHS,

acting as electron mediating units. In addition, it was predicted theoretically<sup>9a</sup> and shown experimentally<sup>9d</sup> that the oxidation of the copper centers in a double helicate leads to shorter Cu...Cu distances, and thus greater electronic communication in the oxidized form. These observations might explain the enhancement in the anodic signal shown in our extended helicates structure (EHS). The reverse process (reduction of Os<sup>III</sup> to Os<sup>II</sup>; Figure 7, arrow) cannot be attained by the Cu<sup>II</sup> centers ( $E_c = -0.094$  V). The reduction of the Os<sup>III</sup> complexes can only take place at the ITO surface and is limited to the complexes that diffused through the EHS. The EHS mediated ET processes are therefore unidirectional and have the characteristic of a rectifier.<sup>18</sup>

In order to gain additional insight into this unidirectional electron transfer, the potentials of bare ITO, the **1**-based monolayer and the EHS were scanned in the presence of [Os(bpy)<sub>3</sub>](PF<sub>6</sub>)<sub>2</sub> from the onset potential of Os<sup>II</sup>. This experiment effectively narrows the scanning window from -0.4–1.0 V to 0.1–1.0 V (Figure 8A–C, black dashed lines).

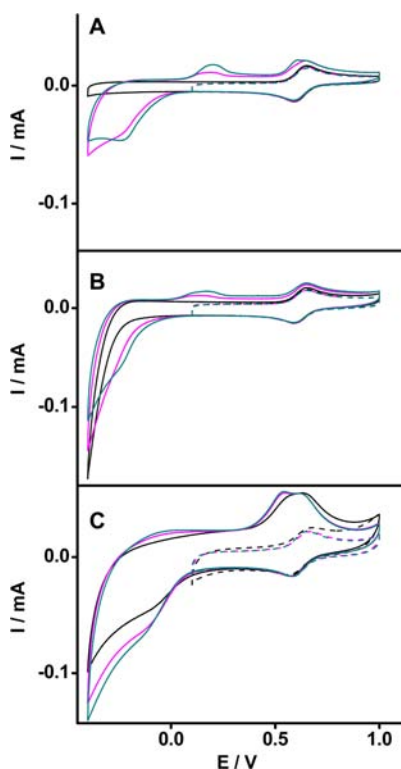


**Figure 8.** Cyclic voltammograms (CVs) of bare ITO electrode (A), and ITO substrates functionalized with (B) the **1**-based monolayer, and (C) the EHS in the presence of [Os(bpy)<sub>3</sub>](PF<sub>6</sub>)<sub>2</sub> (50 μM) and Cu(NO<sub>3</sub>)<sub>2</sub> (0 μM, black; 13 μM, pink; 20 μM, green). The measurements were performed in the ranges of 0.1–1.0 V (dashed lines) and -0.4–1.0 V (solid lines) at 25 °C in argon-degassed KNO<sub>3</sub> electrolyte solutions (0.1 M, vs Ag/AgCl) at 100 mV s<sup>-1</sup>.

No anodic amplification was observed with the EHS in this narrow range (Figure 8C). These experiments were also performed in the presence of different concentrations of Cu(NO<sub>3</sub>)<sub>2</sub> to evaluate effects caused by possible release of copper ions from the helicates to the solutions. As expected, enhancement in the current at 0.18 V was clearly observed upon stepwise increasing the concentration of Cu(NO<sub>3</sub>)<sub>2</sub> from 0 to 20 μM for bare ITO (Figure 8A). This signal is reduced by the **1**-based monolayer (Figure 8B) and significantly less

pronounced when the ITO is functionalized with the EHS (Figure 8C). The effect indicates that the EHS hampers direct contact between the metal-oxide electrode and the copper ions in solution. Interestingly, the Os<sup>III</sup> anodic amplified waves were not significantly different with the EHS upon addition of the Cu(NO<sub>3</sub>)<sub>2</sub> to the solution (Figure 8C). Apparently, this amplification is caused by the surface-bound copper and [Os(bpy)<sub>3</sub>](PF<sub>6</sub>)<sub>2</sub>. Although deposition of Cu(0) cannot be rigorously excluded, anodic stripping with release of copper ions does not appear likely to be at the origin of the amplified anodic wave.

## CONCLUSIONS

We have introduced a multicomponent assembly process to generate surface-bound chiral helicates from solution. This process involves the reaction of two solution-based components to give uniform films. Although operationally it is a one-step procedure, the assembly process is clearly multistep from a mechanistic point of view. The reversible nature of the individual steps, which allows for error-checking, enabled the helicates to be extended uniformly. Mechanistically, the extended chiral helicates are most probably formed in solution prior to binding to the substrates' surfaces.<sup>9,10</sup> Multicomponent assembly processes from solution leading to complex surface-confined structures are relatively rare. For examples, Schaaf and co-workers reported recently the one-pot formation of polymeric films from substrate surfaces triggered by an electrochemically process.<sup>19</sup> Oligomeric and layered metal-organic structures are often formed using stepwise procedures, including Layer-by-Layer (LbL) deposition.<sup>6,20</sup> Our approach can be considered as a new method of thin film formation, with possible applications to a wide range of dynamic systems.<sup>10a</sup> Crucially, this method allowed us to sidestep the solubility problems encountered during the attempted preparation of double-helical oligomers and polymers greater than four Cu<sup>I</sup> ions in length<sup>9a</sup> without need for introducing solubilizing tetra(ethylene glycol) groups, the presence of which appears to reduce interchain electron transfer and conductivity.<sup>21</sup> To demonstrate the scope of the surface-coating process, various substrates were used: (i) silicon, quartz, and indium tin oxide (ITO) coated glass substrates functionalized with covalently bound **1**-based monolayer (Scheme 1), (ii) bare hydrophilic substrates, and (iii) silicon and quartz substrates functionalized with hydrophobic pentyl-siloxane monolayers.

The reaction proceeded with retention of molecular information creating extended helical structures in which the coordination core, metal oxidation state, and the chirality of the precursor complexes were preserved. The chirality of the structures was demonstrated by the selective interaction with a neurotransmitter. The close proximity of metal centers in the metallo-polymeric wires and a high degree of electronic delocalization (as predicted by computational studies)<sup>9b</sup> may make this system an interesting testing ground for electron-transfer studies as demonstrated here by the rectifier (diode like) behavior.<sup>18,22</sup>

## EXPERIMENTAL SECTION

**Materials and Methods.** Acetonitrile (anhydrous, 99.98%), DMF (anhydrous, 99.98%), and other chemicals were purchased from Sigma-Aldrich. Compounds **1** and **2**, and the *p*-iodobenzyl-functionalized glass and silicon substrates were prepared and characterized as reported.<sup>23,24</sup> [Os(bpy)<sub>3</sub>](PF<sub>6</sub>)<sub>2</sub> was prepared using a known procedure and was identified by <sup>1</sup>H NMR and mass spectroscopy.<sup>25</sup>

Glass pressure tubes were cleaned by immersion in a piranha solution (7:3 v/v H<sub>2</sub>SO<sub>4</sub>/30% H<sub>2</sub>O<sub>2</sub>) for 10 min, followed by deionized (DI) water and then acetone. Subsequently, the tubes were oven-dried overnight at 130 °C. (*Caution: piranha solution is an extremely dangerous oxidizing agent and should be handled with care using appropriate personal protection.*) Indium tin oxide (ITO) and single-crystal silicon (100) substrates (Wafernet, San Jose, CA) were cleaned by sonication for 8 min sequentially in *n*-hexane, acetone, and ethanol and then dried under a stream of N<sub>2</sub>. Next, the slides were treated with a UVOCS cleaning system (Montgomery, PA), washed with ethanol, dried under a stream of N<sub>2</sub>, and heated overnight at 130 °C in an oven. Quartz slides (ChemGlass, 2.5 × 0.8 × 0.1 cm<sup>3</sup>) were rinsed with DI water and cleaned by immersion in a piranha solution (7:3 v/v H<sub>2</sub>SO<sub>4</sub>/30% H<sub>2</sub>O<sub>2</sub>) for 1 h (see the above warning). The substrates were then rinsed with DI water followed by the RCA cleaning protocol solution: 1:5:1 (v/v) NH<sub>3</sub>·H<sub>2</sub>O/H<sub>2</sub>O/30% H<sub>2</sub>O<sub>2</sub> at room temperature for 1 h. Next, the substrates were washed with DI water and isopropanol, dried under an N<sub>2</sub> stream, and heated overnight at 130 °C. Transmission UV/vis spectra were recorded on glass or quartz slides with a Cary 100 spectrophotometer using the double beam mode. Atomic force microscopy (AFM) images were recorded using a Solver P47 (NT-MDT, Russia) operated in the semicontact/tapping scanning mode. The ~100 μm silicon cantilevers were used with a resonant frequency of 70–90 kHz. The roughness values, R<sub>rms</sub>, were obtained from 500 nm × 500 nm images using silicon substrates. Several areas with different scanning size were analyzed (1 × 1 μm<sup>2</sup>, 3 × 3 μm<sup>2</sup> and 500 × 500 nm<sup>2</sup>). Film thicknesses were estimated using a J. A. Woollam (Lincoln, NB) model M-2000 V variable angle spectroscopic ellipsometer with VASE32 software. Measurements were performed on silicon for each 5° in a range of 50°–80° over wavelengths of 399–1000 nm. Parameters A, B, and C were 1.45, 0.01, and 0.00, respectively, with MSE < 10 for a Cauchy model. The SiO<sub>2</sub> layer was calibrated to be 17 Å. Circular dichroism (CD) spectra were recorded on an Applied Photophysics Chirascan Circular Dichroism Spectrophotometer (Applied Photophysics Ltd., UK) using quartz slides over a wavelength range of 200–600 nm at 20 °C with a 3-nm bandwidth and 1.0-nm data intervals. Raw data were corrected using the baseline of untreated quartz substrates.

**Angle Resolved X-ray Photoelectron Spectroscopy (AR-XPS).** These measurements were performed at the University of Catania, Italy. Films on silicon and quartz substrates were measured at five different takeoff angles relative to the surface plane (5°, 15°, 30°, 45°, 80°) with a PHI 5600 MultiTechnique System (base pressure of the main chamber 2 × 10<sup>-10</sup> Torr). The acceptance angle of the analyzer and the precision of the sample holder concerning the takeoff angle are ±3° and ±1°, respectively. Samples were mounted on Mo stubs and were excited with Al K $\alpha$  radiation. The silicon slides were radiated using a monochromator. High-resolution spectra of C(1s), O(1s), Si(2p), N(1s), Cu(2p), and Cl(2p) were collected with 5.85 eV pass energy and resolutions of better than 0.3 and 0.5 eV for silicon and quartz, respectively. The structure resulting from satellite K $\alpha$  radiation was subtracted from the spectra of quartz slides, radiated with the unmonochromatized source, before data processing. The XPS peak intensities were obtained after removing the Shirley background. The C(1s) line at 285.0 eV was used for calibration. For details regarding data analysis, see ref 26.

**Specular X-ray Reflectivity (XRR).** These measurements were performed at beamline X6B of the National Synchrotron Light Source (Brookhaven National Laboratory, U.S.) using a four-circle Huber diffractometer in the specular reflection mode (i.e., the incident angle  $\theta_{in}$  was equal to the exit angle  $\theta_{ex}$  and the wave vector transfer  $|\mathbf{q}| = q_z = (4\pi/\lambda) \sin \theta$  is along the surface normal) and the position sensitive linear detector. X-rays of energy of  $E = 10.0$  keV ( $\lambda = 1.24$  Å) were used for these measurements. The beam size was 0.30 mm vertically and 0.5 mm horizontally. The samples were held under a helium atmosphere during the measurements to reduce radiation damage and background scattering from the ambient gas. The off-specular background was measured and subtracted from the specular counts. The sample preparation and the XRR measurements were performed

at ambient laboratory temperatures, which ranged from 20 to 25 °C. For details regarding data analysis, see refs 12 and 27.

X-ray data were also collected at the 12-BM-B beamline at the Advanced Photon Source (APS) in the Argonne National Laboratory (Argonne, IL). In addition to conventional XRR method, the in-plane XRD method was applied for determination of possible lateral periodicity and ordering of molecules in a film. For in-plane XRD measurements, the parallel monochromatic X-ray beam was incident on the sample at angle,  $\theta_{in}$ , of 0.10°, which was set to be smaller than the critical angle of total reflection of 0.18° for silicon substrate. Scattered X-ray intensity was monitored in such grazing incidence geometry in a lateral direction as a function of angle  $\psi$ . X-rays of energy  $E = 10$  keV ( $\lambda = 1.24$  Å) were used for these measurements. The beam size was 0.40 mm vertically and 0.60 mm horizontally. The samples were placed under helium during measurements to reduce background scattering and radiation damage. The sample preparation and the XRR measurements were performed at ambient laboratory temperature, which ranged between 20 and 25 °C. Details of the data acquisition and analysis are given elsewhere.<sup>12,27</sup> The in-plane XRD measurements show a diffraction peak at  $q_{xy} = 0.366$  Å<sup>-1</sup> (Figure 3B) that can be assigned to the lateral ordering. The mean intermolecular spacing  $\bar{a}$  and the mean long-range dimension  $L$  (the characteristic size of the ordered regions), along the surface direction, were calculated as:  $\bar{a} = 2\pi/q_{xy,max}$ ;  $L = 0.9\lambda/(\beta \cos \psi_{max})$ , where  $\beta$  is the full width at one-half of the maximum intensity of the Bragg peak observed at a scattering angle of  $\psi_{max}$  and  $q_{xy,max}$  is the reciprocal space coordinate of the Bragg peak.

**Electrochemical Measurements.** A potentiostat (CHI660A) in a three-electrode cell configuration was used consisting of (i) a modified ITO (working electrode), (ii) a Pt wire (counter electrode), and (iii) Ag/AgCl (a reference electrode). The experiments were performed at room temperature after degassing the cell with argon in (i) a phosphate buffer electrolyte solution (0.1 M, pH = 7.4), (ii) a phosphate buffer electrolyte solution (0.1 M, pH 7.4) with [Os(bpy)<sub>3</sub>](PF<sub>6</sub>)<sub>2</sub> (50 μM) or in (iii) KNO<sub>3</sub> electrolyte solutions (potential ranges of -0.4–1.0 V and 0.1–1.0 V). Experiments were also performed in KNO<sub>3</sub> electrolyte solutions (0.1 M, pH = 5.0) in the presence of Cu(NO<sub>3</sub>)<sub>2</sub> (7 μM, 13 μM, 20 μM) and [Os(bpy)<sub>3</sub>](PF<sub>6</sub>)<sub>2</sub> (50 μM).

**Monolayer Formation with Helicate 1.** *p*-Iodobenzyl-functionalized quartz, ITO, and silicon substrates were immersed in a dry acetonitrile/DMF (9:1, v/v) solution of helicate 1 (0.40 mM) in a glass pressure tube under N<sub>2</sub> (SI Scheme S1). The sealed tubes were heated at 50 °C for 96 h with exclusion of light. Subsequently, the slides were sonicated consecutively at room temperature in acetonitrile/DMF (8:2, v/v) for 5 min (× 2), 5 min in ethanol, carefully cleaned with Kimwipes (wetted with ethanol), and then dried under a stream of N<sub>2</sub>.

**Formation of Pentyl-Siloxane Monolayers.** Freshly cleaned silicon and quartz substrates were treated with a dry toluene solution of pentyltrichlorosilane (2.1 mM) at room temperature for 2 h under N<sub>2</sub> to provide siloxane-based monolayers. The substrates were then rinsed in dry toluene (4×) and sonicated in toluene, in CH<sub>2</sub>Cl<sub>2</sub> for 5 min, and in ethanol for 3 min, and dried under a stream of N<sub>2</sub>. Aqueous CA measurements showed the formation of a hydrophobic surface with  $\theta = 90^\circ$ . The monolayer thickness is 0.8 nm as observed by ellipsometry.

**Formation of Extended Helicate Structures (EHS).** Substrates functionalized with the 1-based monolayer ( $\theta = 30^\circ$ ), clean hydrophilic substrates ( $\theta = 35^\circ$ ), and substrates functionalized with a hydrophobic pentyl-siloxane monolayer ( $\theta = 90^\circ$ ) were loaded into a glass pressure vessel. Then, these substrates were immersed in a D<sub>2</sub>O solution of helicate 1 and with an aqueous solution of 1,2-diaminobenzene. The final concentrations of helicate 1 and 1,2-diaminobenzene were 0.40 mM and 3.70 mM, respectively. The pressure vessel was heated for five days at 50 °C under N<sub>2</sub> with the exclusion of light. The substrates were then sonicated for 5 min in DI water (× 2), sonicated in ethanol for 3 min and then dried under a stream of N<sub>2</sub>. The substrates were stored in air with exclusion of light at room temperature.

**Formation of Extended Helicate Structures (EHS) from 4-Subcomponents.** The 1-based monolayers were loaded into a glass pressure vessel and immersed into a 6 mL D<sub>2</sub>O solution of 1,10-phenanthroline-2,9-dicarboxaldehyde (1.7 mM), 1,2-phenylenediamine (3.4 mM), (S)-3-amino-1,2-propanediol (8.0 mM), copper(I) tetrakis(acetonitrile) tetrafluoroborate (1.9 mM) and heated for five days at 50 °C under N<sub>2</sub> with the exclusion of light. The films were then sonicated for 5 min in DI water (× 2), sonicated in ethanol for an additional 5 min and then dried under a stream of N<sub>2</sub>. The samples were stored in air with exclusion of light at room temperature. The thickness as obtained by ellipsometry was 10 nm.

## ■ ASSOCIATED CONTENT

### ● Supporting Information

Scheme S1 and Figures S1–S11. This material is available free of charge via the Internet at <http://pubs.acs.org>.

## ■ AUTHOR INFORMATION

### Corresponding Author

[jrn34@cam.ac.uk](mailto:jrn34@cam.ac.uk); [milko.vanderboom@weizmann.ac.il](mailto:milko.vanderboom@weizmann.ac.il)

### Notes

The authors declare no competing financial interest.

## ■ ACKNOWLEDGMENTS

This research was supported by the Helen and Martin Kimmel Center for Molecular Design, a Weizmann-UK collaborative grant, the EC FP7 Initial Training Network “DYNAMOL” by the U.S. National Science Foundation (DMR-1006432), and by the Center for Electrical Energy Storage, an Energy Frontier Research Center funded by the U.S. Department of Energy, Office of Science, Office of Basic Energy Sciences, under Contract No. DE-AC02-06CH11357. A.G. thanks the FIRB project ITALNANONET (RBPRO5JH2P). M.B. is the incumbent of the Bruce A. Pearlman Professorial Chair in Synthetic Organic Chemistry.

## ■ REFERENCES

- (1) (a) Newton, G. N.; Onuki, T.; Shiga, T.; Noguchi, M.; Matsumoto, T.; Mathieson, J. S.; Nihei, M.; Nakano, M.; Cronin, L.; Oshio, H. *Angew. Chem., Int. Ed.* **2011**, *50*, 4844. (b) Marschall, M.; Reichert, J.; Weber-Bargioni, A.; Seufert, K.; Auwärter, W.; Klyatskaya, S.; Zoppellaro, G.; Ruben, M.; Barth, J. V. *Nature Chem.* **2010**, *2*, 131. (c) Mal, P.; Breiner, B.; Rissanen, K.; Nitschke, J. R. *Science* **2009**, *324*, 1697. (d) Ruben, M.; Rojo, J.; Romero-Salguero, F. J.; Uppadine, L. H.; Lehn, J.-M. *Angew. Chem., Int. Ed.* **2004**, *43*, 3644.
- (2) (a) Northrop, B. H.; Zheng, Y.-R.; Chi, K.-W.; Stang, P. J. *Acc. Chem. Res.* **2009**, *42*, 1554. (b) Oliveri, C. G.; Ulmann, P. A.; Wiestner, M. J.; Mirkin, C. A. *Acc. Chem. Res.* **2008**, *41*, 1618.
- (3) (a) Lafferentz, L.; Eberhardt, V.; Dri, C.; Africh, C.; Comelli, G.; Esch, F.; Hecht, S.; Grill, L. *Nat. Chem.* **2012**, *4*, 215. (b) Zacher, D.; Schmid, R.; Wöll, C.; Fischer, R. A. *Angew. Chem., Int. Ed.* **2011**, *50*, 176. (c) Carne, A.; Carbonell, C.; Imaz, I.; Maspocho, D. *Chem. Soc. Rev.* **2011**, *40*, 291. (d) Makiura, R.; Kitagawa, H. *Eur. J. Inorg. Chem.* **2010**, *24*, 3715. (e) Maspocho, D.; Ruiz-Molina, D.; Veciana, J. *Chem. Soc. Rev.* **2007**, *36*, 770.
- (4) (a) Saavedra, H. M.; Mullen, T. J.; Zhang, P.; Dewey, D. C.; Shelley, A.; Weiss, P. S. *Rep. Prog. Phys.* **2010**, *73*, 036501/1. (b) de Ruiter, G.; Motiei, L.; Choudhury, J.; Oded, N.; van der Boom, M. E. *Angew. Chem., Int. Ed.* **2010**, *49*, 4780.
- (5) (a) Liu, B.; Ma, M.; Zacher, D.; Betard, A.; Yusenko, K.; Metzler-Nolte, N.; Wöll, C.; Fischer, R. A. *J. Am. Chem. Soc.* **2011**, *133*, 1734. (b) Eberle, F.; Saitner, M.; Boyen, H.-G.; Kucera, J.; Gross, A.; Romanyuk, A.; Oelhafen, P.; D’Olieslaeger, M.; Manolova, M.; Kolb, D. M. *Angew. Chem., Int. Ed.* **2010**, *49*, 341.
- (6) (a) Liu, B.; Shekhah, O.; Arslan, H.; Liu, J.; Wöll, C.; Fischer, R. A. *Angew. Chem., Int. Ed.* **2012**, *51*, 807–810. (b) Huang, J.; Egan, V.

M.; Guo, H.; Yoon, J.-Y.; Briseno, A. L.; Rauda, I. E.; Garrell, R. L.; Knobler, C. M.; Zhou, F.; Kaner, R. B. *Adv. Mater.* **2003**, *15*, 1158–1161. (c) Nakanishi, T.; Yamakawa, N.; Asahi, T.; Osaka, T.; Ohtani, B.; Uosaki, K. *J. Am. Chem. Soc.* **2002**, *124*, 740–741.

(7) Kuzmenko, I.; Rapaport, H.; Kjaer, K.; Als-Nielsen, J.; Weissbuch, I.; Lahav, M.; Leiserowitz, L. *Chem. Rev.* **2001**, *101*, 1659.

(8) de Ruiter, G.; Lahav, M.; Keisar, H.; van der Boom, M. E. *Angew. Chem., Int. Ed.* **2013**, *52*, 704.

(9) (a) Schultz, D.; Biaso, F.; Frederic, S.; Shahi, A. R. M.; Geoffroy, M.; Rissanen, K.; Gagliardi, L.; Cramer, C. J.; Nitschke, J. R. *Chem.—Eur. J.* **2008**, *14*, 7180. (b) Hutin, M.; Cramer, C. J.; Gagliardi, L.; Shahi, A. R. M.; Bernardinelli, G. R.; Cerny, R.; Nitschke, J. R. *J. Am. Chem. Soc.* **2007**, *129*, 8774. (c) Hutin, M.; Schalley, C. A.; Bernardinelli, G.; Nitschke, J. R. *Chem.—Eur. J.* **2006**, *12*, 4069. (d) Jeffery, J. C.; Riis-Johannessen, T.; Anderson, C. J.; Adams, C. J.; Robinson, A.; Argent, S. P.; Ward, M. D.; Rice, C. R. *Inorg. Chem.* **2007**, *46*, 2417.

(10) (a) Rowan, S. J.; Cantrill, S. J.; Cousins, G. R. L.; Sanders, J. K. M.; Stoddart, J. F. *Angew. Chem., Int. Ed.* **2002**, *41*, 898. (b) Campbell, V. E.; de Hatten, X.; Delsuc, N.; Kauffmann, B.; Huc, I.; Nitschke, J. R. *Chem.—Eur. J.* **2009**, *15*, 6138. (c) Delsuc, N.; Hutin, M.; Campbell, V. E.; Kauffmann, B.; Nitschke, J. R.; Huc, I. *Chem.—Eur. J.* **2008**, *14*, 7140.

(11) Filip-Granit, N.; van der Boom, M. E.; Yerushalmi, R.; Scherz, A.; Cohen, H. *Nano Lett.* **2006**, *6*, 2848.

(12) Evmenenko, G.; van der Boom, M. E.; Kmetko, J.; Dugan, S. W.; Marks, T. J.; Dutta, P. J. *Chem. Phys.* **2001**, *115*, 6722.

(13) (a) Gulino, A.; Lupo, F.; Fragalà, M. E.; Lo Schiavo, S. *J. Phys. Chem. C* **2009**, *113*, 13558. (b) Carniato, S.; Roulet, H.; Dufour, G.; Palacin, S.; Barraud, A.; Millii, P.; Nemer, I. *J. Phys. Chem.* **1992**, *96*, 7072.

(14) Lin, W.; Lee, T.-L.; Lyman, P. F.; Lee, J.; Bedzyk, M. J.; Marks, T. J. *J. Am. Chem. Soc.* **1997**, *119*, 2205.

(15) The extinction coefficients of the films are not necessarily similar.

(16) (a) Ram, M. K.; Sundaresan, N. S.; Malhotra, B. D. *J. Phys. Chem.* **1993**, *97*, 11580. (b) Bard, A. J.; Faulkner, L. R. *Electrochemical Methods: Fundamentals and Applications*, 2<sup>nd</sup> ed.; John Wiley & Sons, Inc.: New York, 2001.

(17) Motiei, L.; Kaminker, R.; Sassi, M.; van der Boom, M. E. *J. Am. Chem. Soc.* **2011**, *133*, 14264.

(18) (a) Liu, Y.; Wang, E.; Dong, S. *Electrochem. Commun.* **2011**, *13*, 906. (b) Qin, Y.; Xu, L.; Ren, J.; Liu, Y.; Wang, E. *Chem. Commun.* **2011**, *47*, 8232. (c) Göhler, B.; Hamelbeck, V.; Markus, T. Z.; Kettner, M.; Hanne, G. F.; Vager, Z.; Naaman, R.; Zacharias, H. *Science* **2011**, *331*, 894. (d) Azzaroni, O.; Álvarez, M.; Abou-Kandil, A. I.; Yameen, B.; Knoll, W. *Adv. Funct. Mater.* **2008**, *18*, 3487.

(19) Rydzek, G.; Jierry, L.; Parat, A.; Thomann, J.-S.; Voegel, J.-C.; Senger, B.; Hemmerlé, J.; Ponche, A.; Frisch, B.; Schaaf, P.; Boulmedais, F. *Angew. Chem., Int. Ed.* **2011**, *50*, 4374.

(20) (a) Zhang, X.; Chen, H.; Zhang, H. *Chem. Commun.* **2007**, 1395. (b) Bell, C. M.; Arendt, M. F.; Gomez, L.; Schmeh, R. H.; Mallouk, T. E. *J. Am. Chem. Soc.* **1994**, *116*, 8314. (c) Decher, G. *Science* **1997**, *277*, 1232.

(21) de Hatten, X.; Asil, D.; Friend, R. H.; Nitschke, J. R. *J. Am. Chem. Soc.* **2012**, *135*, 19170.

(22) (a) Sepunaru, L.; Pecht, I.; Sheves, M.; Cahen, D. *J. Am. Chem. Soc.* **2011**, *133*, 2421. (b) Motiei, L.; Lahav, M.; Gulino, A.; Iron, M. A.; van der Boom, M. E. *J. Phys. Chem. B* **2010**, *114*, 14283. (c) Tuccitto, N.; Ferri, V.; Cavazzini, M.; Quici, S.; Zhavnerko, G.; Licciardello, A.; Rampi, M. A. *Nat. Mater.* **2009**, *8*, 41.

(23) Zhu, P.; van der Boom, M. E.; Kang, H.; Evmenenko, G.; Dutta, P.; Marks, T. J. *Chem. Mater.* **2002**, *14*, 4982.

(24) (a) Schultz, D.; Biaso, F.; Shahi, A. R. M.; Geoffroy, M.; Rissanen, K.; Gagliardi, L.; Cramer, C. J.; Nitschke, J. R. *Chem.—Eur. J.* **2008**, *14*, 7180. (b) Hutin, M.; Cramer, C. J.; Gagliardi, L.; Shahi, A. R. M.; Bernardinelli, G. R.; Cerny, R.; Nitschke, J. R. *J. Am. Chem. Soc.* **2007**, *129*, 8774. (c) Hutin, M.; Schalley, C. A.; Bernardinelli, G.; Nitschke, J. R. *Chem.—Eur. J.* **2006**, *12*, 4069.

(25) Johnson, S. R.; Westmoreland, T. D.; Caspar, J. V.; Barqawi, K. R.; Meyer, T. J. *Inorg. Chem.* **1988**, *27*, 3195.

(26) Gulino, A.; Lupo, F.; Fragalà, M. E.; Lo Schiavo, S. J. *Phys. Chem. C* **2009**, *113*, 13558.

(27) (a) Evmenenko, G.; Stripe, B.; Dutta, P. J. *Colloid Interface Sci.* **2011**, *360*, 793. (b) Evmenenko, G.; Yu, C.-J.; Kewalramani, S.; Dutta, P. *Langmuir* **2004**, *20*, 1698.